Application of Fourier series methods for studying tunnelling of electrons out of quantum wells in an electric field

1999 J. Phys.: Condens. Matter 11 5293

(http://iopscience.iop.org/0953-8984/11/27/306)

J. Phys.: Condens. Matter **11** (1999) 5293–5311. Printed in the UK PII: S0953-8984(99)99440-7

Application of Fourier series methods for studying tunnelling of electrons out of quantum wells in an electric field

S Panda, B K Panda† and S Fung

Department of Physics, The University of Hong Kong, Hong Kong, People's Republic of China

Received 17 November 1998, in final form 23 April 1999

Abstract. The electron energy shifts and mean tunnelling lifetimes in a quantum well with different potential profiles under an applied electric field are calculated using Fourier series methods. In the present work, single-rectangular, symmetric double, and diffusion-modified quantum wells have been taken into account. The mean lifetime at high field strength obtained from the time evolution of the wave packets is found to be lower than that obtained from the conventional standing-wave approach.

1. Introduction

Quantum wells (QWs) show great promise for the fabrication of many novel devices such as infrared detectors, semiconductor lasers, and tunnelling devices. In particular, considerable effort has been devoted to the development of the ultrahigh-speed resonant tunnelling diode [1, 2]. Most of these devices, however, operate under an applied electric field, making an understanding of the mean tunnelling lifetime in these devices essential. Since tunnelling is a quantum phenomenon, a wave mechanical treatment is needed [2]. On the other hand, the fundamental aspects of the tunnelling processes can be understood using the QW as a tool, which is the main motivation of this work.

The calculation of the energy levels in a rectangular quantum well has been carried out using the first-principles pseudopotential theory [3]. Recently Vlaev and Contreras-Solorio have employed tight-binding calculations in order to obtain an understanding of the optical transitions between the ground electron and hole states in both single-rectangular and diffusion-modified quantum wells [4]. Although these calculations give more insight into the problem, they are quite complicated to apply. On the other hand, the implementation of the effective-mass equation and the envelope function approximation for studying tunnelling processes is rather simple.

Austin and Jaros in their pioneering work combined the Airy function method with the scattering approach in order to achieve an understanding of the tunnelling process in the single-rectangular quantum well [5–8]. This method calculates the energy shifts and resonance widths at different electric field strengths very accurately. Later the Airy function approach was simplified by Ahn and Chuang [9] to obtain the energy and resonance width directly from the boundary conditions. However, this method deals with Airy functions of complex arguments, and one needs to find the roots of a complex determinant to estimate the

† Now at: Institute of Ion Beam Physics and Materials Research, Research Centre Rossendorf, Postfach 510119, D-01314 Dresden, Germany.

0953-8984/99/275293+19$30.00

energies and resonance widths. Ghatak *et al* further simplified the method by calculating the energy and mean tunnelling lifetimes from the coefficients of Airy functions of real arguments [10]. The transfer matrix method can then be used to extend the Airy function approach so as to obtain energies and lifetimes in a QW with a non-rectangular well [10, 11]. The effect of the barrier effective mass has also been considered in this method and it is found to have a significant effect on the energies, wavefunctions, and mean tunnelling lifetimes [11, 12].

Several alternative numerical approaches such as the finite-difference method [13–15], finite-element method [16], complex-coordinate approach [17], and Fourier series method [18, 19] have been successfully applied to calculate energies and wavefunctions for any form of the QW. In these methods, the solution is obtained over a distance L which is the sum of the well widths and barrier widths. The convergence of energies and wavefunctions is checked by varying L. The boundary condition in this method is that the wavefunction vanishes at both ends of the distance L, which is equivalent to putting two infinite barriers there. Nakamura *et al* have shown that an infinite barrier in the direction of the electric field results in the formation of a triangular potential [16]. In the Schrödinger equation solution, the eigenstates of this triangular well are coupled with the real eigenstates of the QW. As a result of this, it is not straightforward to separate the states that are formed in the triangular well from the real states in the QW [16]. In addition to this, a definite choice of an appropriate value of the L for a particular QW and high electric field strength is not clear in this method.

Although it appears that achieving the correct understanding of the Stark shift is not possible with a numerical method, the presentation of a stabilization graph (SG), which shows energy levels as a function of L [20], gives a clear understanding of the situation. The avoided crossings between stable and continuum states are typical of SGs. Using the Fermi golden rule in the SG, the energies and lifetimes were estimated earlier for different QWs [20, 21]. Although the method of extracting lifetimes from the SG presents more physical insight into the process involved, it suffers from lack of accuracy [20].

Unfortunately the method of estimating quasi-bound energies and lifetimes from the SG is applicable only in the low-electric-field region. With high electric field the quasi-bound energy becomes negative, and there is a finite probability of finding the wavefunction at infinity. In order to obtain oscillations in the wavefunction outside the well region, further care is necessary to remove the effect of the triangular well.

Although the calculation of the energy shifts from the time-independent Schrödinger equation is a correct method, the stationary wavefunctions in this method do not present any field-induced dynamical picture of the electron. For estimating the lifetime of the electron, different characteristic lifetimes such as the hesitation time, passage time, and dwell time have been proposed, using time-dependent analysis [22, 23]. Therefore this method allows for a more complete description of the electron behaviour, especially in the high-electric-field regions.

In our earlier work, the finite-difference scheme was employed to obtain energies, wavefunctions, and lifetimes in different QW structures [14, 15]. Since the plane waves are orthonormalized, the Fourier series in the plane-wave basis set is an attractive method for solving eigenvalue equations in different physical problems. In our earlier work, this method was found to be efficient in calculating the energy shifts in the arbitrary form of the QW under low electric fields [19]. In the present work, we have extended this method in order to obtain the SG, and adopted an accurate method for obtaining energies and lifetimes from it when the applied electric field is low. For high electric field, a fast numerical scheme based on the Fourier series method is developed for solving the time-dependent Schrödinger equation, and then the probability of tunnelling is calculated in order to obtain lifetimes from it.

2. Method

The energies and wavefunctions in a QW are obtained by solving the time-independent BenDaniel–Duke effective-mass equation [24] which adequately takes the position dependence of the effective mass $m^*(z)$ into account in the kinetic energy operator. Under a uniform electric field F it is given as

$$\left[-\frac{\hbar^2}{2}\frac{\partial}{\partial z}\frac{1}{m^*(z)}\frac{\partial}{\partial z}+V(z)+eFz\right]\Psi_n(z)=E_n\Psi_n(z). \tag{2.1}$$

We have used the Fourier series method [18, 19] to solve equation (2.1). In this method the wavefunction $\Psi_n(z)$ is expanded in terms of plane waves as

$$\Psi_n(z)=\sqrt{\frac{1}{L}}\sum_k C_n(k)\mathrm{e}^{\mathrm{i}(2\pi k/L)z} \tag{2.2}$$

where $\mathrm{i}=\sqrt{-1}$. The potential profile of the well $V(z)$ is expanded in a Fourier series as

$$V(z)=\sum_k \mathcal{V}(k)\mathrm{e}^{\mathrm{i}(2\pi k/L)z} \tag{2.3}$$

where the Fourier coefficient $\mathcal{V}(k)$ can be obtained from the inverse Fourier transform:

$$\mathcal{V}(k)=\frac{1}{L}\int_{-L/2}^{L/2} V(z)\mathrm{e}^{-\mathrm{i}(2\pi k/L)z}\,\mathrm{d}z. \tag{2.4}$$

Since $1/m^*(z)$ and eFz are continuous functions of z, they can be expanded in Fourier series with Fourier coefficients $m(k)$ and $f(k)$ respectively. The BenDaniel–Duke expression, equation (2.1), in terms of the Fourier coefficients $C_n(k)$, $\mathcal{V}(k)$, $m(k)$, and $f(k)$, may be expressed as [18, 19]

$$\sum_l H(k-l)C_n(l)=E_nC_n(k) \tag{2.5}$$

where

$$H(k-l)=\frac{\hbar^2}{2}\left(\frac{2\pi}{L}\right)^2 m(k-l)kl+\mathcal{V}(k-l)+f(k-l). \tag{2.6}$$

This equation is expressed in matrix notation as

$$HC_n=E_nC_n. \tag{2.7}$$

The eigenvalues and eigenfunction coefficients are obtained by diagonalizing equation (2.7).

The eigenvalues as a function of L give the stabilization graph (SG) [20, 21]. The important feature of the SG is that it shows avoided crossings between the stable and continuum states. The extraction of the resonance widths from the SG in quantum chemistry problems such as those of electron–atom and electron–molecule scattering was pioneered by Taylor [25] and co-workers. In the standard golden-rule-type formula, the resonance width (Γ) is given by [20, 21]

$$\Gamma=2\pi\rho(E)V_c^2 \tag{2.8}$$

where the interaction term V_c is taken to be half the energy splitting at the pseudo-crossing (L_c) of the SG, and $\rho(E)$ is the density of the continuum states.

This method has been employed to extract the ground-state resonant energy E_r and the resonance width Γ for the QW under a uniform electric field [20, 21]. However, in this method the accurate determination of V_c and $\rho(E)$ is difficult, as they both involve the estimation of an exact L_c and the values of E at this point. In a QW under a low electric field, Γ is expected

to be quite small, as a result of which this method gives less accurate values [20]. Recently, Taylor's group has presented a novel approach for extracting the accurate E_r and Γs from the SG [26]. They have recognized that the density of resonance states calculated near L_c would show a Lorentzian shape, so the resonance peak and its width can be easily extracted from it. However, it is worth mentioning that the extraction of E_r and Γ from the density of states was first carried out by Austin and Jaros a long time ago [5]. In the following, the method for calculating the density of resonance states is described.

The density of resonance states is given by

$$\rho_L(E) = \sum_n \delta(E_n(L) - E) \tag{2.9}$$

where $E_n(L)$ is the box eigenvalue of the system. Since $\rho_L(E)$ is independent of L in any given range ΔL, we can average the right-hand side of equation (2.9) over the parameter L as follows [26]:

$$\langle \rho_L(E) \rangle \approx \frac{1}{\Delta L} \int_{L-\Delta L/2}^{L+\Delta L/2} \mathrm{d}L\ \rho_L(E). \tag{2.10}$$

Substituting equation (2.9) in equation (2.10), we obtain

$$\langle \rho_L(E) \rangle = \frac{1}{\Delta L} \sum_n \int_{L-\Delta L/2}^{L+\Delta L/2} \mathrm{d}L\ \delta(E_n(L) - E). \tag{2.11}$$

We have the relation

$$\int_{-\infty}^{\infty} \mathrm{d}x\ \delta(f - f(x)) = \mathrm{mod}\left(\frac{\mathrm{d}f}{\mathrm{d}x}\right)^{-1}_{f(x)=f}. \tag{2.12}$$

Taking $\Delta L \to \infty$ in equation (2.11) and using the relation (2.12), we obtain

$$\langle \rho_L(E) \rangle = \frac{1}{\Delta L} \sum_n \mathrm{mod}\left(\frac{\mathrm{d}E_n(L')}{\mathrm{d}L'}\right)^{-1}_{E_n(L')=E}. \tag{2.13}$$

The index n sums the derivative of E_n versus L, satisfying the conditions

$$E_n(L') = E \qquad L - \Delta L/2 < L' < L + \Delta L/2. \tag{2.14}$$

In order to decrease the statistical error, we need to take ΔL large enough that the number of eigenvalues $E_n(L')$ satisfying condition (2.14) will be sufficient to produce convergence. We would like to mention here that the equation for the density of states (2.13) is different from that used by Austin and Jaros [5]. In the present case, the contributions from the excited states are included.

The density of resonance states contains contributions from two regions. It exhibits a resonance behaviour near the avoided crossing point L_c and a flat background (B_L), where $E_n(L)$ is described by straight lines:

$$\rho_L(E) = \rho_L^r(E) + B_L. \tag{2.15}$$

$\rho_L^r(E)$ is the expected resonant part which stabilizes, becoming independent of L, and it is described by a Lorentzian. The background is independent of E and L. Thus equation (2.15) can be expressed as

$$\rho_L(E) = \frac{1}{\pi} \frac{\Gamma/2}{(E_r - E)^2 + \Gamma^2/4} + B_L. \tag{2.16}$$

We observe that the inverse of the derivative of the energy levels with respect to L is needed in equation (2.13) to obtain the density of resonance states. The method for calculating the derivatives is described in appendix A.

The stabilization method is applicable only for low electric field strength. For high electric field intensity, a direct solution of equation (2.7) by the matrix diagonalization method will result in the localizing of some of the wavefunctions in the triangular well. Moreover, the diagonalization method fails to include the zero-field structure. It was demonstrated earlier using our finite-difference scheme [14, 15] that the inverse-power method (IPM), which solves for the energy and wavefunction iteratively, produces correct results. However, in the finite-difference method the wavefunction is obtained in position space. It will be interesting to observe whether the Fourier coefficients obtained in the IPM can generate oscillations in the wavefunction outside the well region under a high electric field. From equation (2.7) we can formulate the following coupled equations, which can be solved iteratively to obtain the energy and Fourier coefficients for the wavefunction for the nth state:

$$C_n^{(m)} = [H - IE_n^{(m-1)}]^{-1} C_n^{(m-1)} \tag{2.17a}$$

$$C_n^{(m)} = \frac{C_n^{(m)}}{\langle C_n^{(m)} | C_n^{(m)} \rangle} \tag{2.17b}$$

$$E_n^{(m)} = \langle C_n^{(m)} | H | C_n^{(m)} \rangle. \tag{2.17c}$$

In principle, the starting energy and Fourier coefficients can be chosen arbitrarily. However, we find that the number of iterations is decided by how correct the starting vector is. Therefore we start the iteration process by choosing the energy and Fourier coefficients at zero electric field. In this way we need only three iterations to get converged results.

The mean tunnelling lifetime at high electric field can be calculated from the probability of the electrons tunnelling out of the well [13–15]. The bias is suddenly applied at $t = 0$. The tunnelling probability for a state at an energy E is calculated by projecting the wavefunction at time t with the initial wavefunction at $t = 0$. In the present work, we have considered the ground state to study the tunnelling probabilities:

$$P_E(t) = 1 - \left| \int \Psi_E^*(z, 0) \Psi_E(z, t) \, \mathrm{d}z \right|^2 \tag{2.18}$$

where $\Psi_E(z, 0)$ is the solution of the time-independent equation (2.1) for the ground-state energy E. We can find from equation (2.18) that at $t = 0$, $P_E(t) = 0$, and at large time, the overlap of $\Psi_E(z, t)$ with $\Psi_E(z, 0)$ becomes exceedingly small, with the result that $P_E(t)$ approaches unity. To get $\Psi_E(z, t)$, one has to solve the time-dependent BenDaniel–Duke equation:

$$\left[-\frac{\hbar^2}{2} \frac{\partial}{\partial z} \frac{1}{m^*(z)} \frac{\partial}{\partial z} + V(z) + eFz \right] \Psi_E(z, t) = \mathrm{i}\hbar \frac{\mathrm{d}}{\mathrm{d}t} \Psi_E(z, t). \tag{2.19}$$

The finite-difference approach has been successfully applied to give $\Psi_E(z, t)$ for single-rectangular [12, 13] and diffusion-modified QWs [15]. Assuming a constant effective mass, Bala and Bala applied the Chebyshev polynomial expansion method to calculate $\Psi_E(z, t)$ [27]. We have formulated a computational scheme based on the Fourier series method, in which the effective mass of the barriers is not taken into account. The details of this method are described in appendix B. In this method, $\Psi_E(z, t)$ is expanded in a Fourier series as

$$\Psi_E(z, t) = \sqrt{\frac{1}{L}} \sum_k D^t(k) \mathrm{e}^{\mathrm{i}(2\pi k/L)z} \tag{2.20}$$

where the time dependence is included in the Fourier coefficient $D^t(k)$. In this method, $D(k)$ at t is obtained from the following iterative equation:

$$D^t(k) = \sum_j \sum_l \Lambda(k - j) \exp\left(-\mathrm{i} \frac{\delta t}{\hbar} \left\{ \frac{\hbar^2}{2m^*(0)} \left(\frac{2\pi j}{L} \right)^2 \right\} \right) \Lambda(j - l) D^{t-\delta t}(l) \tag{2.21}$$

where $\Lambda(k)$ is defined as

$$\Lambda(k) = \frac{1}{L}\int_{-L/2}^{L/2} \mathrm{e}^{-(\mathrm{i}/2\hbar)[V(z)+eFz]\delta t}\mathrm{e}^{-\mathrm{i}(2\pi k/L)z}\,\mathrm{d}z. \tag{2.22}$$

Since the electric field is applied at $t = 0$, $D(k)$ at $t = 0$ is taken to be the time-independent ground-state ($n = 1$) wavefunction coefficient $C(k)$ in equation (2.2). Substituting equations (2.2) and (2.20) in equation (2.18), we find

$$P_E(t) = 1 - \left|\sum_k C^*(k)D^t(k)\right|^2. \tag{2.23}$$

In the present work we have taken δt to be 1×10^{-17} s.

In order to demonstrate the potential of the Fourier series method for the calculation of the energy and its width at both low and high electric fields, we have chosen three different types of QW structure, namely the single-rectangular quantum well (RQW), the symmetric double quantum well (SDQW), and the annealing-induced diffusion-modified quantum well (DMQW). We present our results and compare them with the Airy function approach in the next section.

3. Results and discussion

3.1. The single-rectangular quantum well

The Stark shifts and resonance widths have been thoroughly studied in the single-RQW using different analytic and numerical techniques [9, 10, 12–16, 18–20]. We therefore calculate the mean tunnelling lifetimes for this well to verify the correctness of our calculation. The potential profile for a single-RQW is given by

$$V(z) = \begin{cases} V_0 & \text{for } |z| \geqslant l/2 \\ 0 & \text{for } |z| < l/2 \end{cases} \tag{3.1}$$

where $V_0 = B_{off}[E_g(x) - E_g(0)]$ and l is the width of the well. $E_g(x)$ and $E_g(0)$ are the band gaps of $Al_xGa_{1-x}As$ and GaAs respectively. B_{off} is the band offset, usually taken to be 0.7. The expressions for $E_g(x)$ and $m^*(x)$ at room temperature were given in our earlier work [14]. The width of the well is taken to be 100 Å, and $x = 0.353$ which corresponds to the barrier height of 340 meV. The potential profile $V(z)$ under the application of the electric field is shown in figure 1. At zero electric field intensity, there are three bound states in this well corresponding to energies of 33.70 meV, 134.11 meV, and 289.88 meV.

At the field intensity 250 kV cm^{-1}, the energy levels calculated as a function of L are shown in figure 2. The avoided crossings between stable and unstable eigenvalues at different values of L_c for both the ground-state and the first-excited-state energy levels are clear in this figure. For the calculation of the density of resonance states we need to find the derivatives of the energies with respect to L. We present analytical methods for doing this in appendix A. The calculated derivatives are shown in figure 3. The strength of the inverse of the derivatives decreases with increasing quantum level. Therefore the summation in equation (2.13) is convergent, and we needed only ten avoided crossing points to obtain an accurate density of states. To produce figure 4, we first subtracted the constant background from the density of resonance states and then fitted it with a Lorentzian to obtain E_r and Γ. We repeated this procedure for the electric field at 100 kV cm^{-1}, 150 kV cm^{-1}, 200 kV cm^{-1}, 250 kV cm^{-1}, and present the results in table 1. In order to compare the accuracy of our calculations, we have calculated E_r and Γ in the Airy function approach where the barrier effective mass is

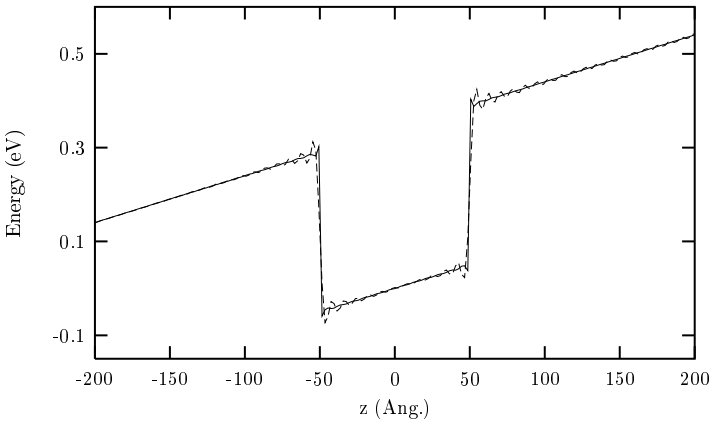

Figure 1. Potential profiles of the single-rectangular quantum well under a uniform electric field. The potential profiles are calculated using equations (2.3), (2.4), and (3.1), where $x = 0.353$, $l = 100$ Å, $B_{off} = 0.7$, and $F = 100$ kV cm^{-1}. The dashed curve and the solid curve are the potential profiles calculated using 101 and 901 plane waves respectively.

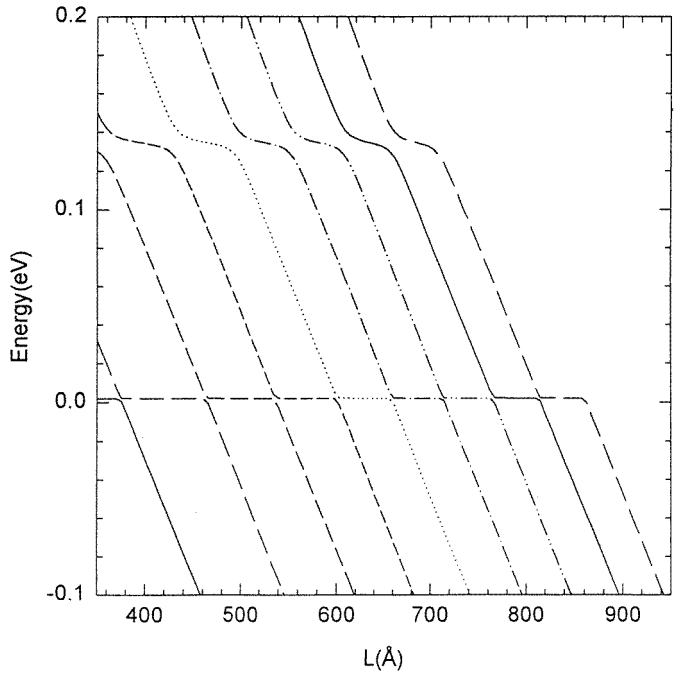

Figure 2. The stabilization graph of the single-rectangular quantum well with well width 100 Å and $x = 0.353$ at the applied field strength 250 kV cm^{-1}. The energy levels for the ground, first, second, third, fourth, fifth, and sixth excited states are denoted by solid, long-dashed, medium-dashed, short-dashed, dotted, dot–dashed, dot–dot–dashed, solid, and long-dashed curves respectively. The avoided crossings are clearly seen here. The avoided crossings for the ground and first exited states are shown here.

incorporated [12], and present the results in table 1. From table 1 it is clear that the present technique for extracting E_r and Γ from the SG is in good agreement with the exact method.

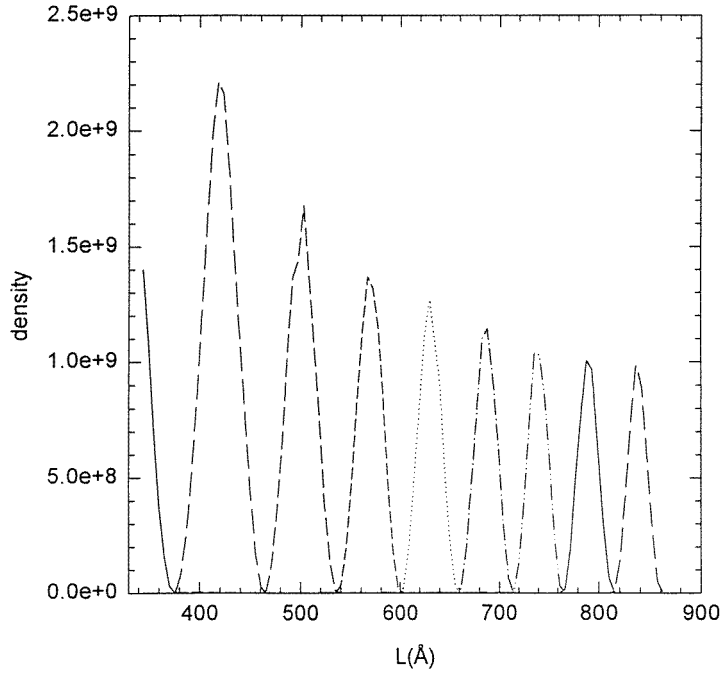

Figure 3. The inverse of the derivative of the ground-state energy levels versus L for the SG shown in figure 2.

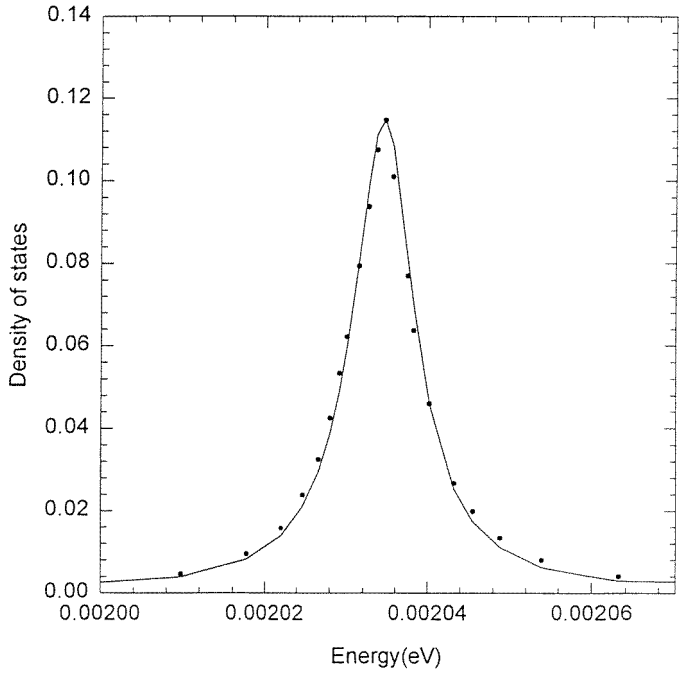

Figure 4. The density of resonance states with the fitted Lorentzian for the ground state of the single-rectangular quantum well. The calculated density of resonance states and the fitted Lorentzian are shown by solid dots and the solid curve respectively.

Table 1. Comparison of the ground-state energy E_r and tunnelling rate Γ for a single-rectangular quantum well in the stabilization and Airy function methods.

	Stabilization method		Airy function method	
F (kV cm^{-1})	E_r (meV)	Γ (meV)	E_r (meV)	Γ (meV)
100	28.176	1.214×10^{-12}	28.117	1.055×10^{-12}
150	21.461	4.154×10^{-9}	21.461	4.357×10^{-9}
200	12.672	3.175×10^{-7}	12.637	3.206×10^{-7}
250	2.097	1.239×10^{-6}	2.187	1.255×10^{-6}

The energy levels calculated at higher field strength using the IPM are compared with the Airy function method in table 2. Unlike in the case of the low electric field intensity, the energies are not so accurately estimated in the IPM for higher field strength. Since the particle starts tunnelling out of the well at high electric field, it requires a large L in our calculation. This in turn needs a large number of plane waves for convergence. In our calculation we have used 901 plane waves, which are not sufficient to achieve convergence. In order to demonstrate this, the ground-state wavefunctions calculated in the Airy function method and the IPM at 350 kV cm^{-1} are shown in figure 5. We find that there is a slight disagreement between these two methods. In order to reproduce exact energies at the field strengths 300 kV cm^{-1} and 350 kV cm^{-1}, we need to use 1201 and 1501 plane waves respectively.

Table 2. Comparison of the ground-state energy E_r in the single-rectangular quantum well in the inverse-power and Airy function methods. The ground-state Γs are calculated from the wave-packet solution and compared with those obtained in the Airy function method.

	This work		Airy function method	
F (kV cm^{-1})	E_r (meV)	Γ (meV)	E_r (meV)	Γ (meV)
300	-9.751	1.596×10^{-3}	-10.160	8.071×10^{-4}
350	-22.811	2.322×10^{-3}	-23.719	1.312×10^{-3}
400	-36.463	5.224×10^{-3}	-38.455	3.030×10^{-3}

The probability of tunnelling $P_E(t)$ for the ground-state energy E is shown in figure 6 for field strengths of 300 kV cm^{-1} and 400 kV cm^{-1}. We find that it initially shows oscillations, and then reaches a steady state. Oleinik and Arepjev have presented a numerical method in order to give an understanding of the behaviour of the wave packets in a rectangular well under an electric field applied only on one side of the well [28]. They have described how the sudden application of the bias produces an intense shaking of the system. The electrons are largely knocked out of the initial stationary state, passing into continuous spectra states. The wave packets formed by the continuous spectra states are spread out over time. However, after a short interval of time the wave packet can be described by a superposition of the quasi-stationary states with finite lifetimes. The oscillations in $P_E(t)$ arise from the interference of the transition amplitudes corresponding to the electron jumping from the level E to the neighbouring levels. The period of the oscillations in $P_E(t)$ may be understood in terms of the classical frequency of the wave packet, which arises from the superposition of the quasi-stationary states in the QW [29]. The tunnelling of the electron through the barrier takes place through the bound electron states in the well. The physical situation in the present case is qualitatively the same as that described above.

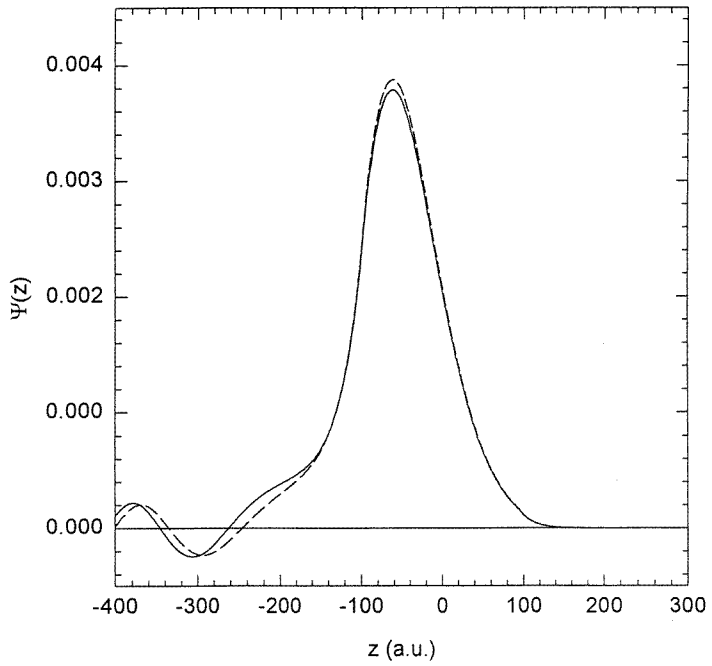

Figure 5. The ground-state wavefunction of the single-rectangular well in the inverse-power and Airy function methods under an applied electric field of 350 Å are shown as solid and dashed curves respectively.

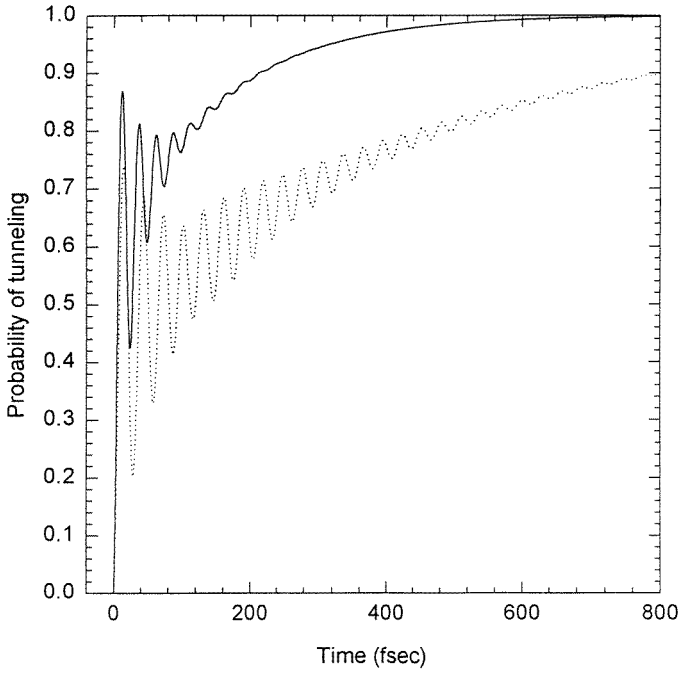

Figure 6. The tunnelling probabilities at 300 kV cm^{-1} and 400 kV cm^{-1} are shown by the dotted curve and solid curve respectively.

For long times the probability may be described as $P(t) = 1 - \exp(-\Gamma t)$. For different field strengths, the resonance widths are tabulated in table 2. For comparison, we have evaluated Γ using the Airy function approach where the barrier effective mass is not taken into account. We find that in this calculation the resonance widths are longer than those obtained from the exact method. Since the process of the tunnelling of the electron in this analysis is different from those in the Airy function approach which utilizes stationary waves, the mean tunnelling lifetimes are different. It needs more elaborate analysis to understand this difference. One possibility is that the electrons go to higher quasi-bound states in the wave packet and thus need less time to tunnel out of the well.

3.2. The symmetric double quantum well

In the present section we study the RDQW, which has the potential profile

$$V(z) = \begin{cases} 0 & \text{for } h/2 < |z| < l + h/2 \\ V_0 & \text{for } |z| \leqslant h/2 \\ V_0 & \text{for } |z| \geqslant l + h/2 \end{cases} \tag{3.2}$$

where l and h are the width of the well and the separation distance between the two symmetric wells. The potential profile calculated taking $l = 60$ Å, $h = 40$ Å, $x = 0.353$, and $F = 100$ kV is shown in figure 7. At zero electric field strength, we obtain four energy levels, namely, 68.17 meV, 70.99 meV, 257.23 meV, and 276.50 meV. The ground-state and first-excited-state energy levels in a single-RQW with width 60 Å are 68.98 meV and 263.61 meV respectively. Due to the interaction of the two wells in the SDQW, the energy level first reduces by the shift integral term and then the degeneracy is lifted by the transfer integral term [2]. The symmetric and antisymmetric combinations of the transfer integrals give rise to two closely spaced energy levels. The energy levels at 68.98 meV in the single-RQW give rise to the two energy levels 68.17 meV and 70.99 meV, and the first-excited-state energy level 264.61 meV gives rise to the energy levels 257.23 meV and 276.50 meV. The analytic expressions for calculating the resonance widths from the SG are given in appendix A. The resonance positions and widths of the ground-state energy levels calculated from the SG for different field intensities are

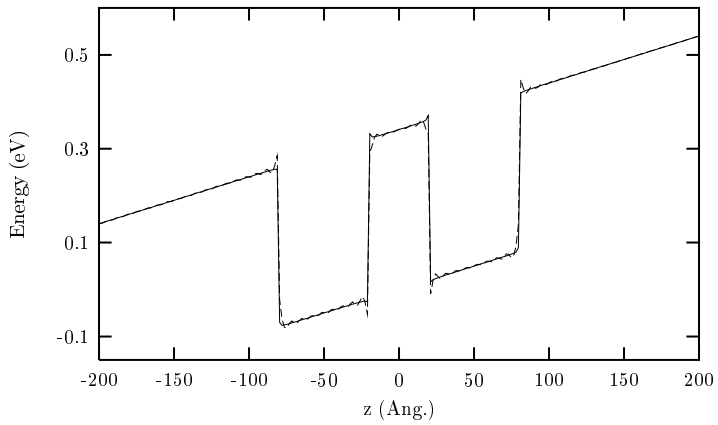

Figure 7. Potential profiles of the symmetric double quantum well under a uniform electric field. The width of the well and the separation length between wells are 60 Å and 40 Å respectively. The other parameters are the same as for figure 1. The dashed and solid curves are calculated using 201 and 1201 plane waves respectively.

shown in table 3. We obtain excellent agreement between the present stabilization and Airy function methods. The energy level decreases very quickly with increasing field strength. The resonance widths are found to be very small in this well. Unlike in the single-RQW where the particle encounters only one barrier region, in the present case the particle needs to tunnel through two barrier regions, and so it requires a longer time to escape.

Table 3. Comparison of the ground-state E_r and Γs for the symmetric double quantum well calculated in the stabilization and the Airy function methods. The resonance width at 80 kV cm^{-1} is too small to be accurately calculated in the stabilization method.

	Stabilization method		Airy function method	
F (kV cm^{-1})	E_r (meV)	Γ (meV)	E_r (meV)	Γ (meV)
80	28.177		28.050	1.373×10^{-17}
100	17.581	1.898×10^{-14}	17.351	2.376×10^{-14}
120	6.887	5.853×10^{-12}	6.753	3.491×10^{-12}

The quasi-bound energies for higher field strengths calculated using the IPM are compared with those obtained by the exact method in table 4. Unlike in the case of the single-RQW, we find good agreement between these two methods for this well using only 901 plane waves. Since the tunnelling time is quite short, the method does not require a large number of plane waves as it does for the single-RQW.

Table 4. Comparison of the ground-state E_r for the symmetric double quantum well in the inverse-power and Airy function methods. The ground-state Γs are calculated from the wave-packet solution and compared with those obtained in the Airy function method.

	This work		Airy function method	
F (kV cm^{-1})	E_r (meV)	Γ (meV)	E_r (meV)	Γ (meV)
150	−9.484	8.963×10^{-10}	−9.552	4.963×10^{-10}
180	−26.986	6.337×10^{-8}	−25.052	1.337×10^{-8}
200	−37.140	9.906×10^{-8}	−37.151	6.906×10^{-8}

The probability of tunnelling is shown in figure 8 for field strengths of 150 kV cm^{-1} and 200 kV cm^{-1}. It shows oscillations as in the single-RQW. The difference is that $P_E(t)$ approaches unity during the initial oscillations. This results from the tunnelling of the wave packet at the barrier between the two wells. At long times, the probability decreases from unity, showing that the effect of the barrier between two wells reduces on the tunnelling of the wave packet out of the well. The calculated resonance widths are compared with those obtained from the Airy function method and presented in table 4. As in the case of the single-RQW, we find that the resonance widths are larger in the wave-packet tunnelling scheme.

3.3. The diffusion-modified quantum well

When the RQW is subjected to annealing above 800 °C, intermixing starts at the hetero-junction, and the formation of Ga vacancies induces Al atoms to diffuse into the GaAs layer from the AlGaAs region [30, 31]. The interdiffusion process is therefore characterized by the Al diffusion length ($L_d = \sqrt{Dt}$) which can be obtained from the diffusion constant (D) at the annealing temperature and annealing time (t). Taking the diffusion constant to be isotropic,

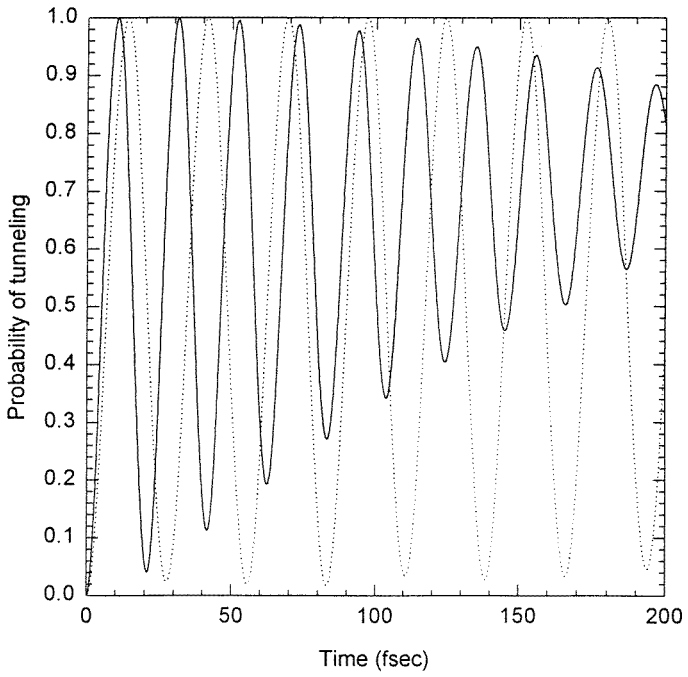

Figure 8. The tunnelling probabilities at 150 kV cm^{-1} and 200 kV cm^{-1} are shown by the dotted curve and solid curve respectively.

the position-dependent Al concentration is found from the diffusion equation as [30, 31]

$$w(z) = x\left[1 - \frac{1}{2}\left\{\mathrm{erf}\left(\frac{l+2z}{4L_d}\right) + \mathrm{erf}\left(\frac{l-2z}{4L_d}\right)\right\}\right] \tag{3.3}$$

where erf is the error function [32] and l is the width of the rectangular QW. The potential profile is expressed as

$$V(z) = B_{off}[E_g(w(z)) - E_g(w(0))]. \tag{3.4}$$

We have taken $x = 0.353$, $l = 100$ Å, and $L_d = 20$ Å. The potential profiles with and without an electric field are shown in figure 9. We have carried out the integration for calculating $\mathcal{V}(k)$ and $m(k)$, respectively, using the fast Fourier transform method, as the analytic integrations are difficult in this case. The derivatives of the functions $\mathcal{V}(k)$ and $m(k)$ with respect to L are also taken numerically. The ground-state energies and resonance widths for different field intensities are presented in table 5. The energies agree with our earlier calculation based on the finite-difference method [15]. However, the resonance widths are different, as the earlier results were based on time-dependent analysis. The resonance width increases very quickly with increasing electric field compared to that in the single-RQW under the same electric field. This happens as a result of the less abrupt shape of the tunnelling barrier.

The energy levels for higher field strengths obtained from the IPM are tabulated in table 6. We find that our results are in poor agreement with those computed in the Airy function approach for high electric field. However, the results can be improved by including more plane waves. The resonance widths obtained from the wave-packet tunnelling without taking the barrier effective mass into account are found to be slightly larger than those obtained in the Airy function method.

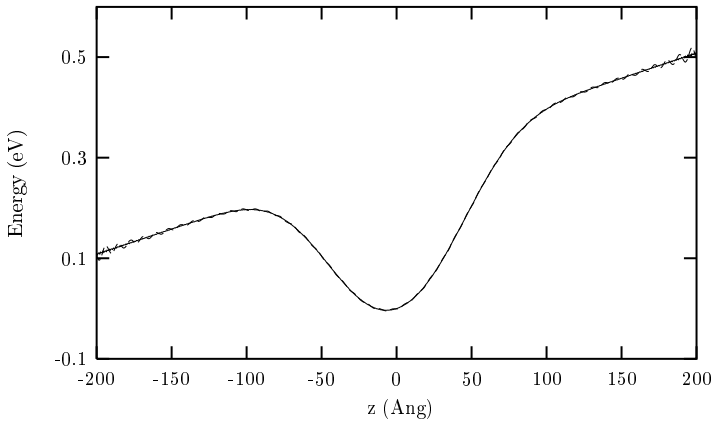

Figure 9. Potential profiles of the diffusion-modified quantum well under a uniform electric field of intensity 100 kV cm^{-1}. The width of the well is taken to be 100 Å and the diffusion constant (L_d) =20 Å. The other parameters are the same as for figure 1. The dashed curve and solid curve are the potential profiles calculated using 91 and 401 plane waves respectively. In this case a large number of plane waves are not necessary to achieve convergence because of its non-abrupt barrier.

Table 5. Comparison of the ground-state E_r and Γs for the single diffusion-modified quantum well calculated in the stabilization and the Airy function methods.

	This work		Airy function method	
F (kV cm^{-1})	E_r (meV)	Γ (meV)	E_r (meV)	Γ (meV)
100	55.489	1.889×10^{-10}	55.521	2.362×10^{-10}
150	49.918	1.381×10^{-6}	49.936	1.445×10^{-6}
200	41.761	2.120×10^{-4}	41.653	2.071×10^{-4}
250	30.557	1.342×10^{-3}	30.193	1.250×10^{-3}
300	15.340	6.170×10^{-3}	15.265	5.793×10^{-3}

Table 6. Comparison of the ground-state E_r in the diffusion-modified quantum well in the inverse-power and Airy function methods. The ground-state Γs are calculated from the wave-packet solution and compared with those obtained in the Airy function method.

	This work		Airy function method	
F (kV cm^{-1})	E_r (meV)	Γ (meV)	E_r (meV)	Γ (meV)
350	−2.152	2.720×10^{-2}	−2.071	1.519×10^{-2}
400	−19.214	5.811×10^{-2}	−20.466	1.520×10^{-2}
450	−30.841	2.104×10^{-1}	−38.957	4.598×10^{-2}

4. Conclusions

In the present work we have applied the Fourier series method to calculate the ground-state quasi-bound energy levels together with their resonance widths in the rectangular, symmetric double, and diffusion-modified QWs under low and high electric field. In our time-dependent Schrödinger equation, we are unable to incorporate the barrier effective mass. However, the present wave-packet solution scheme is an order of magnitude faster than our previous scheme

based on the finite-difference method [15]. The probability of tunnelling gives more insight into the tunnelling process caused by the impact of a sudden bias than the lifetimes calculated from it. For low electric fields we have observed the collapse and revival of the wave packets; this is at variance with the recent analysis by Bluhm *et al* [29]. Work is in progress with the aim of finding an explanation of this feature.

Appendix A. Evaluation of the derivatives of the eigenvalues

The energy eigenvalues are generally calculated from wavefunctions as

$$E_n = \int \Psi_n^*(z) H(z) \Psi(z)\, \mathrm{d}z. \tag{A.1}$$

Substituting equation (2.2) in equation (A.1) we obtain

$$E_n = \sum_k \sum_{k'} C_n^*(k) H(k-k') C_n(k'). \tag{A.2}$$

Since we find that $C_n(k)$ does not depend on L, we take the derivative only of $H(k-k')$:

$$\frac{\partial E_n}{\partial L} = \sum_k \sum_{k'} C_n^*(k) \left[\frac{\partial H(k-k')}{\partial L} \right] C_n(k'). \tag{A.3}$$

We can find from equation (2.6) that

$$\frac{\partial H(k-k')}{\partial L} = -\frac{2}{L} m(k-k') k k' \left(\frac{2\pi}{L} \right)^2 + \left(\frac{2\pi}{L} \right)^2 k k' \frac{\partial m(k-k')}{\partial L} + \frac{\partial \mathcal{V}(k-k')}{\partial L} + \frac{\partial f(k-k')}{\partial L}. \tag{A.4}$$

We need to evaluate the Fourier coefficients $m(k)$, $\partial m(k)/\partial L$, $\partial \mathcal{V}(k)/\partial L$, and $\partial f(k)/\partial L$ to calculate equation (A.4). The Fourier coefficient $m(k)$ is defined as

$$m(k) = \frac{1}{L} \int_{-L/2}^{L/2} \frac{1}{m^*(z)} \mathrm{e}^{-\mathrm{i}(2\pi k/L)z}\, \mathrm{d}z. \tag{A.5}$$

The Fourier coefficient of the uniform electric field is given by

$$f(k) = \frac{eF}{L} \int_{-L/2}^{L/2} z \mathrm{e}^{-\mathrm{i}(2\pi k/L)z}\, \mathrm{d}z. \tag{A.6}$$

Solving this exact integral, we obtain

$$f(k) = -\frac{\mathrm{i}}{2} eFL y_0(\pi k) \tag{A.7}$$

where $y_0(x) = \cos(x)/x$. The derivative of $f(k)$ with respect to L is given by

$$\frac{\partial f(k)}{\partial L} = -\frac{\mathrm{i}}{2} eF y_0(\pi k). \tag{A.8}$$

A.1. The single-rectangular quantum well

$\mathcal{V}(k)$ for the single-RQW is obtained by substituting equation (3.1) in equation (2.4):

$$\mathcal{V}(k) = V_0 \left[j_0(\pi k) - \frac{l}{L} j_0\left(\pi k \frac{l}{L} \right) \right] \tag{A.9}$$

where $j_0(x)$ is the spherical Bessel function of 0th order. The derivative $\partial\mathcal{V}(k)/\partial L$ is obtained as

$$\frac{\partial\mathcal{V}(k)}{\partial L} = V_0\frac{l}{L^2}\cos\left(\pi k\frac{l}{L}\right). \tag{A.10}$$

The Fourier coefficient of the effective mass $m(k)$ in this well is derived as

$$m(k) = \left[\frac{1}{m^*(x)} - \frac{1}{m^*(0)}\right]\frac{l}{L}j_0\left(\pi k\frac{l}{L}\right) + \frac{1}{m^*(0)}j_0(\pi k). \tag{A.11}$$

The derivative of $m(k)$ is found from equation (A.11) as

$$\frac{\partial m(k)}{\partial L} = \left[\frac{1}{m^*(x)} - \frac{1}{m^*(0)}\right]\frac{l}{L^2}\cos\left(\pi k\frac{l}{L}\right). \tag{A.12}$$

A.2. The symmetric double quantum well

Substituting equation (3.2) in equation (2.4) we find $V(k)$ for the SDQW as follows:

$$V(k) = V_0\left[j_0(\pi k) + \frac{h}{L}j_0\left(\pi k\frac{h}{L}\right) - \frac{2l+h}{L}j_0\left(\pi k\frac{2l+h}{L}\right)\right]. \tag{A.13}$$

The derivative is obtained as

$$\frac{\partial V(k)}{\partial L} = V_0\left[\left(\frac{2l+h}{L^2}\right)\cos\left(\pi k\frac{2l+h}{L}\right) - \frac{h}{L^2}\cos\left(\pi k\frac{h}{L}\right)\right]. \tag{A.14}$$

$m(k)$ for this well is obtained as

$$m(k) = \left[\frac{2l+h}{L}j_0\left(\pi k\frac{2l+h}{L}\right) - \frac{h}{L}j_0\left(\pi k\frac{h}{L}\right)\right]\left[\frac{1}{m^*(0)} - \frac{1}{m^*(x)}\right] + \frac{1}{m^*(x)}j_0(\pi k). \tag{A.15}$$

The derivative of $m(k)$ is found to be

$$\frac{\partial m(k)}{\partial L} = \left[\frac{1}{m^*(x)} - \frac{1}{m^*(0)}\right]\left[\left(\frac{2l+h}{L^2}\right)\cos\left(\pi k\frac{2l+h}{L}\right) - \frac{h}{L^2}\cos\left(\pi k\frac{h}{L}\right)\right]. \tag{A.16}$$

The Fourier coefficients of $V(k)$, $m(k)$, and their derivatives for the single-RQW are reproduced by taking $h = 0$ and $2l = l$ in the corresponding expressions for the SDQW.

Appendix B. Solution of the time-dependent Schrödinger equation

The solution of the time-dependent BenDaniel–Duke expression, equation (2.19), is given by [33]

$$\Psi_E(z, t+\delta t) = \exp\left(-\frac{\mathrm{i}}{\hbar}\left[-\frac{\hbar^2}{2}\frac{\partial}{\partial z}\frac{1}{m^*(z)}\frac{\partial}{\partial z} + V(z) + eFz\right]\delta t\right)\Psi_E(z, t). \tag{B.1}$$

The kinetic and potential energy operators are separated as follows:

$$\Psi_E(z, t+\delta t) = \exp\left(-\frac{\mathrm{i}}{\hbar}\left[-\frac{\hbar^2}{2}\frac{\partial}{\partial z}\frac{1}{m^*(z)}\frac{\partial}{\partial z}\right]\delta t\right)\exp\left(-\frac{\mathrm{i}}{\hbar}[V(z) + eFz]\,\delta t\right)\Psi_E(z, t). \tag{B.2}$$

However, equation (B.2) violates the Baker–Campbell–Hausdorff (BCH) theorem [33] which states that

$$\mathrm{e}^A\mathrm{e}^B = \mathrm{e}^{A+B+C_1+C_2+\cdots} \tag{B.3}$$

where $C_1 = \frac{1}{2}[A, B]$, $C_2 = \frac{1}{12}([A, [A, B]] - [B, [A, B]])$. Since the kinetic energy operator does not commute with the potential energy operator, C_1, C_2, and all higher-order C_s have non-zero values. However, if δt is sufficiently small, we can adopt the split-operator formalism [33, 34] in order to express equation (B.2) as

$$\Psi_E(z, t + \delta t) = \exp\left(-\frac{\mathrm{i}}{2\overline{h}}[V(z) + eFz]\,\delta t\right)\exp\left(-\frac{\mathrm{i}}{\overline{h}}\left[-\frac{\overline{h}^2}{2}\frac{\partial}{\partial z}\frac{1}{m^*(z)}\frac{\partial}{\partial z}\right]\delta t\right) \times \exp\left(-\frac{\mathrm{i}}{2\overline{h}}[V(z) + eFz]\,\delta t\right)\Psi_E(z, t). \tag{B.4}$$

The ground-state wavefunction at $t = 0$ is expressed in the Fourier series as

$$\Psi_E(z, 0) = \sqrt{\frac{1}{L}}\sum_k C(k)\mathrm{e}^{\mathrm{i}(2\pi k/L)z}. \tag{B.5}$$

We first operate with the potential energy term on $\Psi_E(z, 0)$ in equation (B.4), and define this as

$$\Phi(z) = \mathrm{e}^{-(\mathrm{i}/2\overline{h})[V(z)+eFz]\delta t}\Psi_E(z, 0). \tag{B.6}$$

Since $\Phi(z)$ is continuous with z, we can expand it in a Fourier series as

$$\Phi(z) = \sum_k \phi(k)\mathrm{e}^{\mathrm{i}(2\pi k/L)z}. \tag{B.7}$$

Substituting (B.5) in (B.6) and performing an inverse Fourier transform, we calculate $\phi(k)$ as

$$\phi(k) = \sum_j C(j)\Lambda(k - j) \tag{B.8}$$

where $\Lambda(k)$ is defined as

$$\Lambda(k) = \frac{1}{L}\int_{-L/2}^{L/2}\mathrm{e}^{-(\mathrm{i}/2\overline{h})[V(z)+eFz]\delta t}\mathrm{e}^{-\mathrm{i}(2\pi k/L)z}\,\mathrm{d}z. \tag{B.9}$$

The kinetic energy part is then used to operate on $\Phi(z)$:

$$\Xi(z) = \exp\left(-(\mathrm{i}\,\delta t/\overline{h})\left[-\frac{\overline{h}^2}{2}\frac{\partial}{\partial z}\frac{1}{m^*(z)}\frac{\partial}{\partial z}\right]\delta t\right)\Phi(z). \tag{B.10}$$

The function $\Xi(z)$ can be expanded in a Fourier series:

$$\Xi(z) = \sum_k \xi(k)\mathrm{e}^{\mathrm{i}(2\pi k/L)}. \tag{B.11}$$

Since δt is exceedingly small, we can expand the kinetic energy operator in equation (B.10) in Taylor's series:

$$\sum_k \xi(k)\mathrm{e}^{\mathrm{i}(2\pi k/L)z} = \left[1 - \mathrm{i}\frac{\delta t}{\overline{h}}\left(-\frac{\overline{h}^2}{2}\frac{\partial}{\partial z}\frac{1}{m^*(z)}\frac{\partial}{\partial z}\right) + \cdots\right]\sum_l \phi(l)\mathrm{e}^{\mathrm{i}(2\pi l/L)z}. \tag{B.12}$$

On simplification, we obtain

$$\xi(k) = \phi(k) - \mathrm{i}\frac{\delta t}{\overline{h}}\left[\frac{\overline{h}^2}{2}\left(\frac{2\pi}{L}\right)^2\sum_l m(k - l)\phi(l)kl + \cdots\right]. \tag{B.13}$$

The evaluation of the higher-order terms in this equation involves more convolution terms. Taking $m(k - l) = m^*(0)\delta_{kl}$ and substituting in (B.13), we obtain

$$\xi(k) = \phi(k)\left[1 - \mathrm{i}\frac{\delta t}{\overline{h}}\left\{\frac{\overline{h}^2}{2m^*(0)}\left(\frac{2\pi k}{L}\right)^2\right\} + \cdots\right] = \phi(k)\exp\left(-\mathrm{i}\frac{\delta t}{\overline{h}}\left\{\frac{\overline{h}^2}{2m^*(0)}\left(\frac{2\pi k}{L}\right)^2\right\}\right). \tag{B.14}$$

Finally we proceed to operate with the potential energy on $\xi(z)$:

$$\Psi(z, \delta t) = \mathrm{e}^{-(\mathrm{i}/2\overline{h})[V(z)+eFz]\delta t}\xi(z). \tag{B.15}$$

We can expand $\Psi(z, \delta t)$ as

$$\Psi(z, \delta t) = \sqrt{\frac{1}{L}}\sum_k D(k)\mathrm{e}^{\mathrm{i}(2\pi k/L)z}. \tag{B.16}$$

Using equation (B.9) we can obtain $D(k)$ as

$$D(k) = \sum_j \xi(j)\Lambda(k-j). \tag{B.17}$$

Combining equations (B.8), (B.14), and (B.17), we find the solution of equation (B.4) to be as follows:

$$D(k) = \sum_j \sum_l \Lambda(k-j)\exp\left(-\mathrm{i}\frac{\delta t}{\overline{h}}\left\{\frac{\overline{h}^2}{2m^*(0)}\left(\frac{2\pi j}{L}\right)^2\right\}\right)\Lambda(j-l)C(l). \tag{B.18}$$

To get $D(k)$ for the time step $2\,\delta t$, we must replace $C(l)$ in (B.8) by $D(l)$ obtained for the time step δt. This procedure is then repeated to find $D(k)$ for all time steps.

B.1. The single-rectangular quantum well

For the single-RQW, the expression for $\Lambda(k)$ may be derived by substituting equations (3.1) in equation (B.9) as follows:

$$\begin{aligned}\Lambda(k) = {} & \frac{l}{L}j_0\left[\left(\pi k + \frac{eFL}{4\overline{h}}\,\delta t\right)\frac{l}{L}\right] \\ & + \mathrm{e}^{-\mathrm{i}(V_0/2\overline{h})\delta t}\left[j_0\left(\pi k + \frac{eFL}{4\overline{h}}\delta t\right) - \frac{l}{L}j_0\left[\left(\pi k + \frac{eFL}{4\overline{h}}\,\delta t\right)\frac{l}{L}\right]\right].\end{aligned} \tag{B.19}$$

B.2. The symmetric double quantum well

For the SDQW, $\Lambda(k)$ may be derived by substituting equation (3.2) in equation (B.9) as follows:

$$\begin{aligned}\Lambda(k) = {} & \frac{2l+h}{L}j_0\left(\left(\pi k + \frac{eFL}{4\overline{h}}\,\delta t\right)\frac{2l+h}{L}\right) - \frac{h}{L}j_0\left(\left(\pi k + \frac{eFL}{4\overline{h}}\,\delta t\right)\frac{h}{L}\right) \\ & + \mathrm{e}^{-\mathrm{i}(V_0/2\overline{h})\,\delta t}\left[j_0\left(\pi k + \frac{eFL}{4\overline{h}}\,\delta t\right) - \frac{2l+h}{L}j_0\left(\left(\pi k + \frac{eFL}{4\overline{h}}\,\delta t\right)\frac{2l+h}{L}\right)\right. \\ & \left. + \frac{h}{L}j_0\left(\left(\pi k + \frac{eFL}{4\overline{h}}\,\delta t\right)\frac{h}{L}\right)\right].\end{aligned} \tag{B.20}$$

Under the conditions $h = 0$ and $l = 2l$, equation (B.20) reproduces equation (B.19).

References

[1] Loehr J P and Manasreh M O 1993 *Semiconductor Quantum Wells and Superlattices for Long Wavelength Infrared Detectors* ed M O Manasreh (Boston, MA: Artech House Publishers) p 19

[2] Bastard G 1988 *Wave Mechanics Applied to Semiconductor Heterostructures* (Les Ulis: Les Editions de Physique)

[3] Hagon J P, Jaros M and Herbert D C 1989 *Phys. Rev.* B **40** 6420

[4] Vlaev S and Contreras-Solorio D A 1997 *J. Appl. Phys.* **82** 3853

[5] Austin E J and Jaros M 1985 *Phys. Rev.* B **31** 5569

[6] Austin E J and Jaros M 1985 *Appl. Phys. Lett.* **47** 274

[7] Austin E J and Jaros M 1987 *J. Appl. Phys.* **62** 558
[8] Austin E J and Jaros M 1988 *Phys. Rev.* **38** 6326
[9] Ahn D and Chuang S L 1986 *Phys. Rev.* B **34** 9034
[10] Ghatak A K, Goyal I C and Gallawa R L 1990 *IEEE J. Quantum Electron.* **26** 305
[11] Hutchings D C 1989 *Appl. Phys. Lett.* **55** 1082
[12] Panda S, Panda B K and Fung S, unpublished
[13] Juang C, Kuhn K J and Darling R B 1990 *Phys. Rev.* B **41** 12 047
[14] Panda S and Li E H 1997 *Superlatt. Microstruct.* **22** 313
[15] Panda S, Panda B K, Fung S and Beling C D 1996 *J. Appl. Phys.* **80** 1532
[16] Nakamura K, Shimizu A, Koshiba M and Hayata K 1989 *IEEE J. Quantum Electron.* **25** 889
[17] Bylecki M, Jaskólski W and Oszwaldowski R 1996 *J. Phys.: Condens. Matter* **8** 6393
[18] Mathine D L, Myjak S K and Maracas G N 1995 *IEEE J. Quantum Electron.* **31** 1216
[19] Panda S, Panda B K, Fung S and Beling C D 1996 *Solid State Commun.* **99** 299
[20] Borondo F and Sánchez-Dehesa J 1986 *Phys. Rev.* B **33** 8758
[21] Proto J A, Sánchez-Dehesa J, Cury L A, Nogare S and Portal J C 1994 *J. Phys.: Condens. Matter* **6** 887
[22] Landauer R and Martin T 1994 *Rev. Mod. Phys.* **66** 217
[23] Imafuku K, Ohba I and Yamanaka Y 1995 *Phys. Lett.* A **204** 329
[24] BenDaniel D J and Duke C B 1966 *Phys. Rev.* **152** 683
[25] Taylor H S 1970 *Adv. Chem. Phys.* **18** 91
[26] Mandelshtam V A, Ravuri T R and Taylor H S 1993 *Phys. Rev. Lett.* **70** 1932
[27] Bala P and Bala W 1995 *Appl. Phys.* A **60** 293
[28] Oleinik V P and Arepjev Ju 1984 *J. Phys. A: Math. Gen.* **17** 1817
[29] Bluhm R, Kostelecky A and Tudose B 1997 *Phys. Rev.* A **55** 819
[30] Chang L L and Koma A 1976 *Appl. Phys. Lett.* **29** 138
[31] Mukai K, Sugawara M and Yamazaki S 1994 *Phys. Rev.* B **50** 2273
[32] *Handbook of Mathematical Functions* 1964 ed M Abramowitz and I A Stegun (Washington, DC: National Bureau of Standards) p 446
[33] de Vries P L 1994 *A First Course on Computational Physics* (New York: Wiley)
[34] Truong T N, Tanner J J, Bala P, McCammon J A, Kouri D J, Lesyng B and Hoffman D 1992 *J. Chem. Phys.* **96** 2077